Soil Dynamics and Earthquake Engineering 85 (2016) 217–230

Contents lists available at ScienceDirect

Soil Dynamics and Earthquake Engineering

journal homepage: www.elsevier.com/locate/soildyn

Analysis of the effect of groundwater level on the seismic behavior of an unsaturated embankment on clayey ground

Takahiro Yoshikawa [a], Toshihiro Noda [b,*], Takeshi Kodaka [c], Toshihiro Takaine [d]

[a] Department of Civil Engineering, Nagoya University, Nagoya, Japan
[b] Disaster Mitigation Research Center, Nagoya University, Nagoya, Japan
[c] Department of Civil Engineering, Meijo University, Nagoya, Japan
[d] GEOASIA Research Society, Nagoya, Japan

ARTICLE INFO

Article history:
Received 27 June 2015
Received in revised form
31 December 2015
Accepted 15 February 2016
Available online 22 April 2016

Keywords:
Soil–water–air coupled analysis
Unsaturated soil
Groundwater level
Elasto-plastic constitutive equation
Finite deformation analysis
Dynamic/static analysis
Clayey soil ground

ABSTRACT

Numerous river levees on clayey soil grounds were damaged by the 2011 off the Pacific coast of Tohoku Earthquake. In order to investigate such damage, the behavior of an unsaturated embankment on clayey ground was simulated during its construction, during an earthquake and after the earthquake. The simulation was carried out using a soil–water–air coupled finite deformation analysis code, with attention being focused on the effect of groundwater level. The results indicated that if the groundwater level is high, a saturated area (settlement-induced saturation area) is formed at the base of the embankment due to penetrative settlement during/after construction. In addition, the mean skeleton stress is low compared with the low groundwater level. As a consequence, in the embankment on ground with the high groundwater level, the co-seismic deformation is greater and the mean skeleton stress decreases sharply, particularly in the settlement-induced saturation area during the earthquake. It was also shown that after the earthquake, the groundwater level rises because water flows toward the unsaturated embankment from the settlement-induced saturation area and/or the saturated clayey ground. If the groundwater level is high, in particular, a phreatic line is formed temporarily within the embankment.

1. Introduction

The off the Pacific coast of Tohoku Earthquake of 11 March 2011 caused massive damage to grounds and earth structures. Damage to river levees was especially prominent and has received much attention. Although liquefaction of sandy foundation grounds has been the focus of attention in investigations of seismic damage to river levees, the earthquake caused collapse of river levees on clayey foundation grounds in several areas. A number of studies [1–3] have suggested that collapse occurs through the following mechanism: deformation of clayey ground during construction of a levee embankment causes settlement of the base of the embankment to below the groundwater level, and this leads to formation of a saturated area at the embankment's base. The saturated area is termed "settlement-induced saturation area" hereafter. The presence of this settlement-induced saturation area, in combination with decreases in the horizontal stress and density of the embankment's base, produces liquefaction of the settlement-induced saturation area during the earthquake and the consequent collapse of the levee embankment. Damage caused by liquefaction of an settlement-induced saturation area had already been pointed out with respect to the collapse of a river levee on peat ground during the 1993 Kushiro-oki Earthquake [4] but came to receive wide attention after the extensive damage caused by the off the Pacific coast of Tohoku Earthquake. Analytical and experimental research have been carried out with the aim of clarifying the mechanism of such damage. In an analytical study, Uzuoka and Semba [5] carried out a soil–water–air coupled finite deformation analysis and compared, before seismic response analysis, the result in which the deformation process during embankment construction is taken into account with the result in which the deformation process is not taken into account. The comparison showed that in the former case, the deformation produced during embankment construction decreases the mean effective stress at the base of the embankment, which results in the deformation produced during and after an earthquake becoming large. The experimental work of Okamura et al. [6] using centrifuge tests to simulate the behavior of an embankment during construction and earthquake showed that a saturated zone is formed at the base of the embankment due to deformation of the foundation

* Corresponding author at: Chikusa, Nagoya, Aichi 464-8603, Japan.
Tel.: +81 52 789 3833.
E-mail address: noda@nagoya-u.jp (T. Noda).

http://dx.doi.org/10.1016/j.soildyn.2016.02.008

ground during construction and that collapse of the embankment is related to the existence of this saturated zone and to the decreases in effective stress and density at the embankment base. A Technical Committee for Study of Restoration Techniques of Levees along the *Kitakamigawa* River and Other Rivers [3] was set up by the Tohoku Regional Development Bureau, Ministry of Land, Infrastructure, Transport and Tourism, to survey and interpret the actual extent of damage to levees caused by the off the Pacific coast of Tohoku Earthquake and propose suitable restoration measures. The committee's report describes the actual conditions and features of the damage, focusing on the microtopography, soil characteristics and groundwater levels. Regarding groundwater levels, the committee's report offers the following statements.

> "It has been observed that in the *Edano* and *Shimonakanome* upstream regions, groundwater is present in the bottom parts of the damaged levee cross sections, whereas groundwater is not present in the bottom parts of the undamaged levee cross sections."
>
> "It has been observed that at 16 locations except the *Sunayama*, *Wadatanuma*, *Kimatsuka*, *Hashiura* and *Nakano* regions, the levels of groundwater present within the levees are equal to or higher than the inland ground heights (or high water bed heights). In contrast, groundwater was not present in the undamaged levee cross sections or the ground water levels were lower than those in the damaged levee cross sections."

Fig. 1 shows the cross section of the *Narusegawa* river levee in the disaster-affected *Shimonakanome* region, 30.0 km upstream of the river mouth. This figure is a partly redrawn version of the one in Sasaki et al. [1]. What is meant by "groundwater is present in the bottom part of the damaged levees" in the abovementioned report is that the groundwater surface was observed to be convex upward within the levee, as can be seen in Fig. 1. It is believed that this groundwater surface was already present before the earthquake. Although research is being carried out to improve the accuracy of simulation of seepage lines that are convex upward, such simulation is considered to be difficult if actual rainfall is used in the seepage analysis [7].

With the above background in mind, this paper utilizes the soil-water-air coupled finite deformation analysis code [8] to numerically simulate the behavior of an unsaturated embankment on clayey foundation ground, focusing attention on the difference in groundwater levels. The behavior during embankment construction, during an earthquake and after the earthquake is simulated as an approach to clarify the mechanism of the damage described above. This analysis code is based on the soil-water coupled finite deformation analysis code [9], which is mounted with the SYS Cam-clay model [10] that allows description of soils ranging from sand through to clay, including even intermediate soils, within the same theoretical framework and is capable of determining deformation and collapse phenomena without distinguishing between dynamic and static behavior. The above code was extended to make it applicable to unsaturated soils as well, and it is capable of handling saturated and unsaturated conditions seamlessly. The two specific cases analyzed were (1) a ground with the groundwater level set to coincide with the ground surface initially (high initial groundwater level) and (2) a ground with the groundwater level set to be 2 m below the ground surface initially (low initial groundwater level). Unsaturated embankments were constructed on the two types of ground, and the calculations were continued until consolidation had ended (i.e., until the excess pore water pressure had completely dissipated), after which seismic response analysis was carried out in order to clarify how the difference in groundwater level affects the mechanical behavior. The existence of a seepage line within the levee before the earthquake was not assumed when setting the initial groundwater level in the current study, unlike in a previous study [7]. This paper shows that when the initial groundwater level is high, a seepage line is formed temporarily within the unsaturated embankment after the earthquake and discusses the mechanism of this phenomenon.

2. Analytical conditions

Fig. 2 is an outline of the cross section analyzed, showing mainly the hydraulic boundary conditions and the air boundary conditions. Assuming two-dimensional plane strain conditions, the cross section was configured by reference to Fig. 1, however, study of alternately layered grounds of clayey and sandy soils or detailed investigations of damaged cross sections of former levees in the *Shimonakanome* region, etc. are not carried out here. The objective of this work was to carry out three-phase finite deformation analysis of unsaturated embankments on clayey grounds under simple conditions and discuss the results thus obtained. The width set for the cross section analyzed is greater than 500 m. Note that the surroundings of the embankment are shown magnified in Fig. 2. Distribution diagrams of strain, stress and other quantities obtained through the analysis are shown in the following sections and in these diagrams, too, the surroundings of the embankment are shown magnified. The hydraulic boundary condition assumed for the ground and embankment surface was that of constant total head (potential head + pressure head), and the air condition was the exhausted condition, i.e., always at atmospheric pressure. All other boundaries were in the undrained and unexhausted condition. Hydraulic boundary conditions of actual ground/embankment surfaces are complicated because rainfall and evaporation repeatedly occur. In this analysis, for simplicity, assuming that a groundwater level becomes constant in a steady state, the constant head hydraulic boundary condition was set. The reference plane for the potential water head was set at the lower end of the analyzed section (engineering bedrock). The analysis was performed for 2 cases. The first case was for the initial groundwater level being coincident with the initial ground surface. This case will be referred to as GL-0m hereafter. The second case was for the initial groundwater level being located 2 m below the initial ground surface, hereafter referred to as GL-2m.

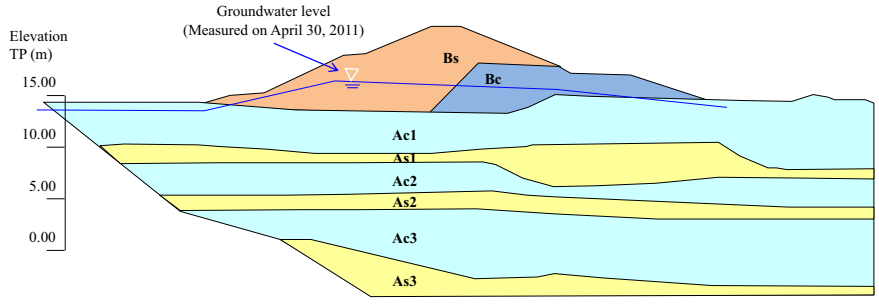

Fig. 1. Cross section of the *Narusegawa* river levee in the disaster-affected *Shimonakanome* region, 30.0 km upstream of the river mouth. (This figure is a partly redrawn version of the one in Sasaki et al., 2012).

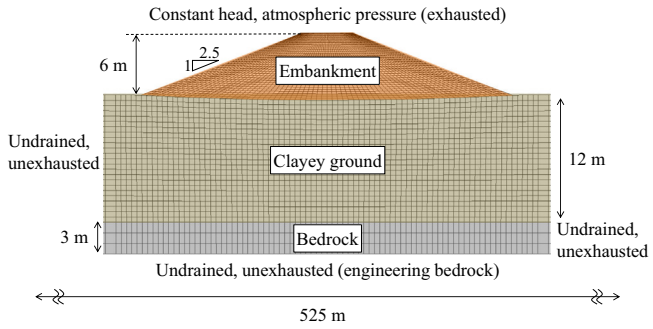

Fig. 2. Cross section used for the analysis showing the hydraulic boundary conditions and the air boundary conditions (the part showing the embankment has been magnified).

The total head of water set for the ground surface and embankment surfaces was 15 m for the first case and 13 m for the second case.

2.1. Material constants and initial conditions set for the clayey ground

The material constants and initial conditions for the clayey ground were decided by simulating with the SYS Cam-clay model [10] the results of undrained triaxial compression tests and constant strain rate consolidation tests carried out on undisturbed samples obtained from an inland location 30.0 km upstream of the mouth of *Narusegawa* river (in the *Shimonakanome* region). The result of the simulation is shown in Fig. 3, and the material constants determined are shown in Table 1. The initial values used for simulating the tests are shown in Table 2. When setting the initial values for the clayey ground, the degree of structure and specific volume were assigned to each layer uniformly from the results of simulation of the undrained triaxial test under a confining pressure of 100 kPa, and the overconsolidation ratio was distributed in the vertical direction according to the overburden pressure [11,12]. The degree of "structure" is an index of soil bulkiness. An example of bulkiness is the high void ratio exhibited by naturally deposited clay under the same stress compared with that of the same clay sufficiently remolded. For details, please refer to the work of Asaoka et al. [10]. The objective of this study is not to reproduce the actual damaged levee in detail. If better reproducibility of soil behavior is needed, additional mechanical tests on disturbed/undisturbed specimens, anisotropic consolidation tests etc. are used. The studies in [13,14] are helpful as the example for determining the material parameters and initial values of SYS Cam-clay model [10]. It has been observed through a separate boring survey that although the foundation ground of *Narusegawa* river was composed predominantly of clayey soil, there were alternating sandy layers in some places and that the clayey soil near these sandy layers contained a high proportion of sand. For this reason, in order to model the clayey foundation ground as a uniform layer of clayey soil, representative values of clay with comparatively high sand content were used in the analyzes. The deep part of the ground was treated as the bedrock, and referring to Tani et al. [15], it was assigned with material constants and initial values of dense sand. The overconsolidation ratio was distributed in the vertical direction according to the overburden pressure as in the case of the clayey ground. Table 3 shows the parameters related to the soil water characteristic curve and other physical properties. The soil water characteristics of the clayey ground and bedrock were decided by referring to the van Genuchten's [16] parameters of silty clay and sand [17], respectively. The Mulaem model [18] was used to obtain the relationships between the degree of saturation and the coefficients of water and air permeability. The initial pore water pressure at the groundwater level was made to coincide with the pore air pressure, and vertically upward from there, a hydrostatic pressure distribution was assumed. At locations deeper than the ground water level, the initial pore air pressure is equal to the water pressure since suction is zero. At locations shallower than the ground water level, the initial pore air pressure was distributed in the vertical direction based on the self-weight of air. The distribution of the initial degree of saturation at locations deeper than the ground water level was calculated according to the hydraulic pressure with consideration to the compressibilities of air and water, assuming that the maximum degree of saturation was at the groundwater level. The distribution at locations shallower than the ground water level was calculated according to the values of suction using the soil water characteristic curve. The specific methods used to calculate the pore water pressure, pore air pressure and degree of saturation of the initial ground are described in the Appendices.

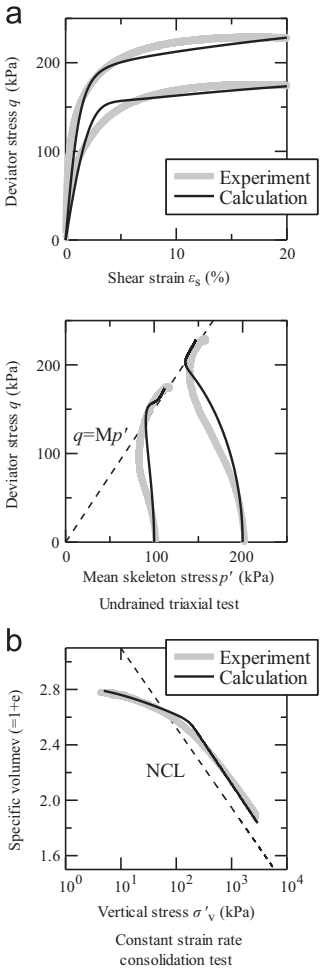

Fig. 3. Experimental and simulated results of an undrained triaxial test and consolidation test on clayey soil specimens.

2.2. Material constants and initial conditions set for the embankment

As it was difficult to obtain the results of mechanical tests using the soil material of the river levees that were damaged by the off the Pacific coast of Tohoku Earthquake, the material constants and initial conditions of the SYS Cam-clay model [10] in the work of Sakai and Nakano [19] were used. The values used in this study are shown in Table 1. The reason for using these parameters was that they had been determined from mechanical tests on soil materials that are actually used for river levees and have sand, silt, and clay contents similar to the material of the damaged levees. The degree of structure and specific volume were assigned to each layer of the embankment

Table 1
Material constants and initial values related to the constitutive equation of the soil skeleton.

		Clayey ground	Bedrock	Embankment
Elasto-plastic parameters				
Specific volume at $q=0$ and $p'=98.1$ kPa on NCL	N	2.45	1.98	1.71
Critical state constant	M	1.5	1.2	1.35
Compression index	$\tilde{\lambda}$	0.25	0.045	0.11
Swelling index	$\tilde{\kappa}$	0.07	0.002	0.02
Poisson's ratio	ν	0.2	0.15	0.3
Evolution rule parameters				
Degradation index of overconsolidation	m	7.0	0.08	0.5
Degradation index of structure	a	0.1	2.2	2.0
Degradation index of structure	b	1.0	1.0	1.0
Degradation index of structure	c	1.0	1.0	1.0
Degradation index of structure	c_s	0.5	1.0	1.0
Evolution index of rotational hardening	b_r	0.1	3.5	0.1
Limit of rotational hardening	m_b	1.0	0.9	0.4
Initial values				
Degree of structure	$1/R^*{}_0$	2.3	1.01	1.2
Overconsolidation ratio	$1/R_0$	6–1400	5000–6500	40–60
Void ratio	e_0	1.39	0.623	0.64
Stress ratio	η_0	0.545	0.545	0.375
Degree of anisotropy	ζ_0	0.545	0.545	0.375

Table 2
Initial values used in the calculations for simulating the mechanical tests on clayey soil specimens.

Initial values		Undrained triaxial test		Constant strain rate consolidation test
		Confining pressure 100 kPa	Confining pressure 200 kPa	
Vertical skeleton stress kPa	σ'_v	100.0	200.0	4.9
Degree of structure	$1/R^*{}_0$	1.47	1.15	2.3
Overconsolidation ratio	$1/R_0$	2.0	1.1	20.0
Void ratio	e_0	1.39	1.28	1.79
Stress ratio	η_0	0.0	0.0	0.0
Degree of anisotropy	ζ_0	0.0	0.0	0.545

Table 3
Material constants and initial values related to the soil–water characteristics and other physical properties.

		Clayey ground	Bedrock	Embankment
Soil–water characteristic curve				
Maximum degree of saturation %	s^w_{max}	99.0	99.0	99.0
Minimum degree of saturation %	s^w_{min}	19.3	10.4	7.32
van Genuchten parameter kPa^{-1}	α	0.051	1.48	0.163
van Genuchten parameter	n'	1.09	2.68	1.37
van Genuchten parameter	m'	0.0826	0.627	0.270
Saturated coefficient of water permeability m/s	k^w_s	5.56×10^{-8}	8.25×10^{-5}	6.94×10^{-7}
Dry coefficient of air permeability m/s	k^a_d	3.06×10^{-6}	4.55×10^{-3}	3.82×10^{-5}
Physical property				
Soil particle density g/cm^3	ρ^s	2.65	2.636	2.67
Bulk modulus of water kPa	K_w	2.19×10^6	2.19×10^6	2.19×10^6
Specific gas constant of air $m^2/s^2/K$	$\bar{R}$	287.04	287.04	287.04
Absolute temperature K	Θ	293.15	293.15	293.15

uniformly, and the overconsolidation ratio was distributed in the vertical direction according to the overburden pressure in a manner similar to the case of ground as described earlier. The embankment was constructed in 30 steps [14] up to a height of 6 m at a rate of 1 m/day. The soil water characteristics of the embankment were decided by referring to the van Genuchten's [16] parameters of silt [17]. The Mulaem model [18] was used to obtain the relationships between degree of saturation and the coefficients of water and air permeability. Fig. 4 depicts the soil water characteristic curve of the embankment and the relationship between degree of saturation and the coefficients of water/air permeability. It can be seen from the relationship between the degree of saturation and the coefficients of water/air permeability that the coefficient of air permeability is greater than that of water permeability up to a degree of saturation of 98.6%. In the following interpretation of the results of the analysis, it is therefore reasonable to assume that air permeation occurs in the embankment before water permeation if the hydraulic gradient and air pressure gradient are of the same level. The initial degree of saturation of the embankment was set at 73.4% [19]. The initial pore air pressure was assumed to be zero, and the initial pore water pressure was determined by calculation from the suction value corresponding to the initial degree of saturation. The state before earthquake was achieved by allowing consolidation after embankment loading to proceed until the excess pore water pressure had completely dissipated.

2.3. Boundary conditions, the input seismic wave, etc.

Fig. 5 illustrates the input seismic wave and its Fourier amplitude spectrum. The north–south component of the seismic waveform observed at KiK-NET *Onoda* (MYGH05, measurement depth 337 m) was modified to correspond to a shear wave velocity of $V_s=300$ m/s using Midorikawa's Equation [20]. Assuming this seismic waveform to be a 2E wave, the E wave was imposed at the bottom boundary of the analyzed cross section in the horizontal direction.

As geometric boundary conditions during embankment construction, it was assumed that the sides of the ground were fixed in the horizontal direction and that the bottom of the ground was fixed in the horizontal and vertical directions. During and after earthquake, it was assumed that, the horizontal direction of the

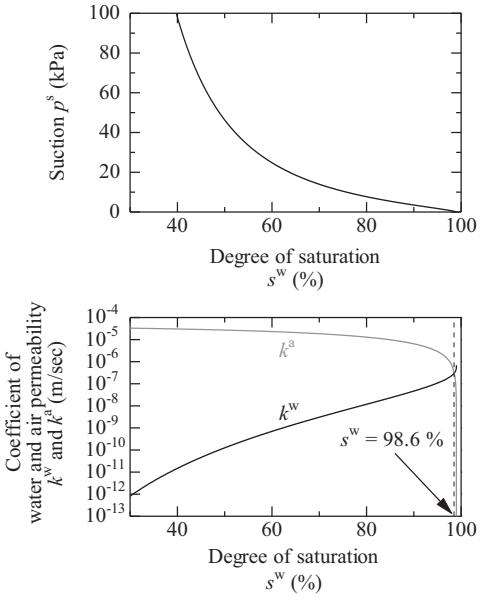

Fig. 4. Soil water characteristic curve of the embankment and the relationship between the degree of saturation and the coefficients of water/air permeability.

bottom of the ground was a viscous boundary [13,21,22] (density $\rho=2.0$ g/cm^3, $V_s=300$ m/s) and that the vertical direction was fixed. Periodic boundaries were assigned to the sides of the ground.

3. Results of analysis of embankment construction

Fig. 6 shows a comparison of the degree of saturation for the cases of (a) groundwater level=GL-0m and (b) groundwater level=GL-2m at the end of consolidation as contour diagrams 20 years after the start of embankment construction. In the case of (a) GL-0m, the total water head of the entire area at the end of consolidation is 15 m because of the hydraulic boundary condition of the total water head of the ground and embankment surfaces being 15 m, as shown in Fig. 2. In other words, the degree of saturation at vertical coordinate positions higher (or lower) than 15 m from the bottom of the analyzed section is lower (or higher) than the maximum degree of saturation. Similarly, the boundary for the maximum degree of saturation is at the 13 m vertical coordinate position in the case of (b) GL-2m. Fig. 7 depicts the mean skeleton stress [23] distributions. The mean skeleton stresses are smaller in the case of GL-0m than GL-2m. This is because the pore water pressures over the whole analyzed cross section are greater in the former case than in the latter case because of the difference in the values of the total water heads set at the ground and embankment surfaces for the two cases.

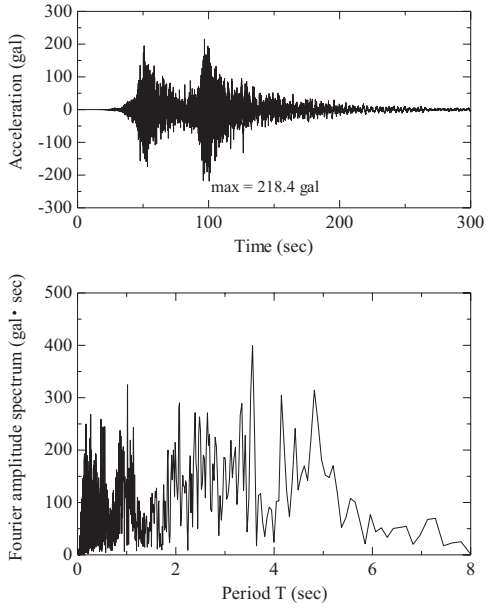

Fig. 5. Seismic waveform input and Fourier amplitude spectrum.

Fig. 8 illustrates the temporal variation of settlement at the center of the base of the embankment. The settlement is greater in the case of GL-0m than GL-2m because the mean skeleton stress is smaller in the former case. Let us now define "saturation" as the condition in which the value of the degree of saturation is greater than the maximum degree of saturation set as a parameter in soil water characteristic curve. Since the final settlement is about 50 cm in the case of GL-0m, a 50 cm "settlement-induced saturation area" is formed at the center of the embankment base. On the other hand, settlement-induced saturation area is not formed in the case of GL-2m because the final settlement was 32 cm. The shapes of the embankment's base (shapes of the ground surface) at the end of the consolidation are shown in Fig. 9, in which dark filled circles indicate the nodes positioned at the toes of slope. The embankment bases exhibit a depression at their centers as a result of the consolidation settlement of the ground. In the case of GL-0m, the ground settled more deeply below than the groundwater level, and this indicates the formation of a settlement-induced saturation area.

4. Results of analysis of co- and post-seismic behavior

The temporal variations in the settlement at the center of the embankment crown in the case of a groundwater level=GL-0m and

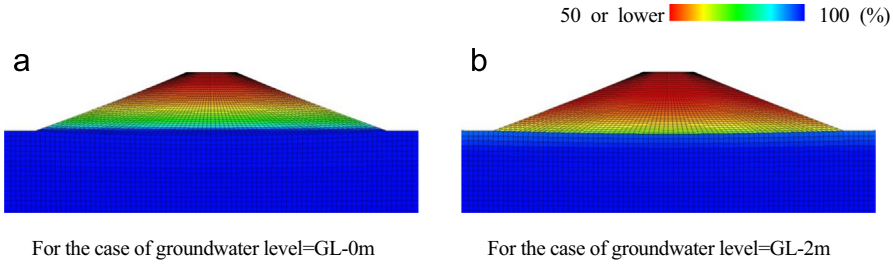

Fig. 6. Distributions of the degree of saturation at the end of the consolidation caused by embankment loading. (a) For the case of groundwater level=GL-0m. (b) For the case of groundwater level=GL-2m.

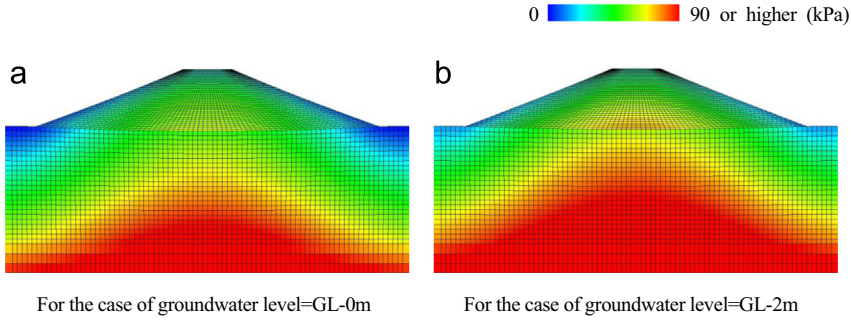

Fig. 7. Mean skeleton stress distributions at the end of the consolidation caused by embankment loading. (a) For the case of groundwater level=GL-0m. (b) For the case of groundwater level=GL-2m.

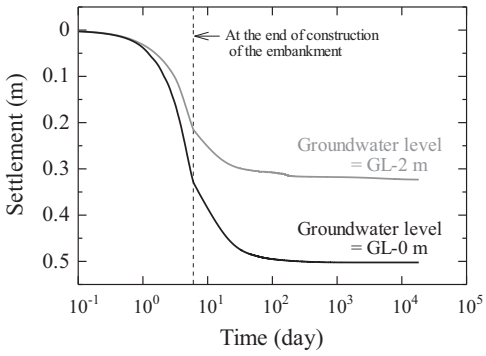

Fig. 8. Comparison of the temporal variation in settlement at the center of the embankment base during its construction.

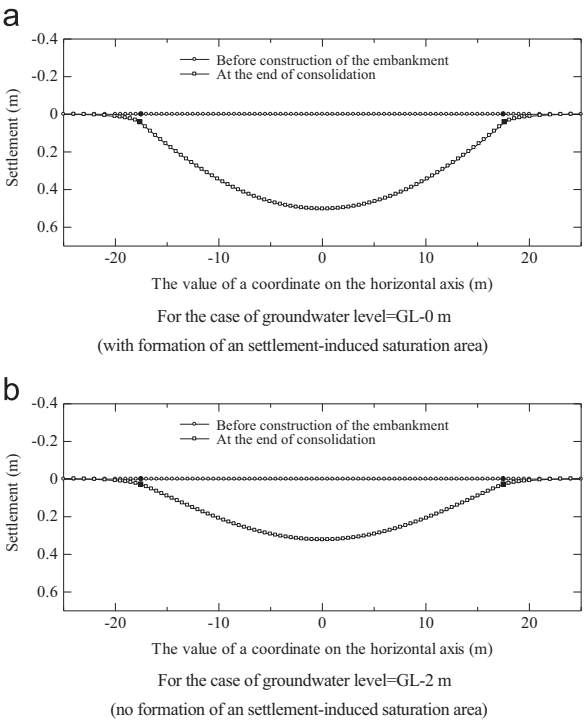

Fig. 9. Shape of the embankment base at the end of the consolidation caused by embankment loading. (a) For the case of groundwater level=GL-0 m. (with formation of an settlement-induced saturation area). (b) For the case of groundwater level=GL-2 m (no formation of an settlement-induced saturation area).

GL-2m are depicted in Figs. 10 and 11, respectively. The settlement is greater in the case of GL-0m, and shaking down settlement exceeding 1 m occurred during the earthquake. In the case of GL-0m as well as GL-2m, the settlement of the embankment during earthquake is large and accounts for a large part of the total crown settlement. The results of the analysis are discussed in detail below in order to clarify the reasons for the difference in the settlement depending on the groundwater level.

The distributions of shear strain, mean skeleton stress, excess pore water pressure and pore air pressure immediately after the earthquake in the cases of GL-0m and GL-2m are compared in Figs. 12–15, respectively. Here, the shear strain ε_s is expressed by $\varepsilon_s = \sqrt{2/3(\boldsymbol{e}' \cdot \boldsymbol{e}')}$, $\boldsymbol{e}' = \boldsymbol{e} - 1/3(\mathrm{tr}\boldsymbol{e})\boldsymbol{I}$, $\boldsymbol{e} = 1/2\left(\boldsymbol{I} - \boldsymbol{B}^{-1}\right)$, and $\boldsymbol{B} = \boldsymbol{F}\boldsymbol{F}^{\mathrm{T}}$ ($\boldsymbol{I}$, identity tensor; $\boldsymbol{F}$, deformation gradient tensor of soil skeleton). The excess pore water pressure is defined as the value generated in excess of the hydrostatic pressure that corresponds to the set groundwater level. Looking at the shear strain distributions in Fig. 12 first, it can be seen that for GL-0m, large shear deformation occurred and that the deformation was concentrated particularly at the base of

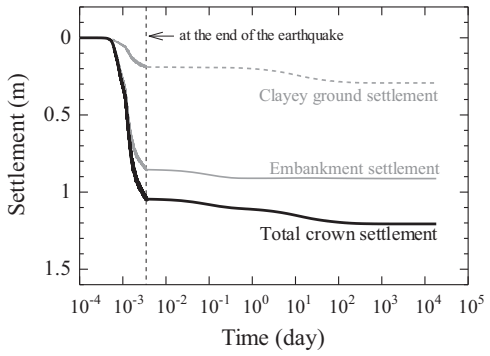

Fig. 10. Temporal variation in the settlement at the center of the embankment crown during and after the earthquake for the case of groundwater level=GL-0m.

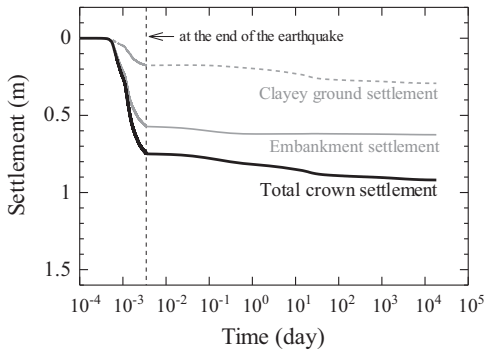

Fig. 11. Temporal variation in the settlement at the center of the embankment crown during and after the earthquake for the case of groundwater level=GL-2m.

the embankment. Fig. 13 shows that when compared with the case GL-2m, the mean skeleton stress for GL-0m is smaller overall, the values being markedly small particularly at the embankment base. Such small values are not seen in the case of GL-2m. The excess pore water pressure and pore air pressure distributions in Figs. 14 and 15 show that although the values at the embankment base are large in the case of GL-0m and GL-2m, the values rose markedly in the case of GL-0m. This is because the mean skeleton stress is small in the case of GL-0m, and an settlement-induced saturation area is present at the embankment base, as shown in Section 3. The mean skeleton stress decreases and the pore water and air pressures increase because shearing in the settlement-induced saturation area during an earthquake takes place under conditions close to constant volume.

The co-seismic mechanical behaviors of the soil element in which the largest shear strain appeared in the cases of GL-0m and GL-2m are illustrated in Figs. 16 and 17, respectively. In these figures, R, R^*, and $\|\boldsymbol{\beta}\|/m_b$ are quantities related to overconsolidation, structure (level bulkiness of the soil) and anisotropy, respectively. For details, please refer to the work of Asaoka et al. [10]. The circles denote the states just before the earthquake. The locations of the output soil elements are indicated in Fig. 12. Although the position of the element in the case of GL-0m differed from that in the case of GL-2m, the locations of the two elements were bilaterally symmetric at the time of embankment construction. Looking at the behavior of the soil element in the case of GL-0m first, shear strains greater than 40% appeared, and the mean skeleton stress decreased to 10 kPa. The degree of saturation remained above the maximum degree of saturation of 99%. Because the degree of saturation was high and water was unable to migrate under short-term external forces due to the earthquake, almost no volume change occurred. Because of this, the pore water and air pressure increased due to the decrease in the mean skeleton stress resulting from plastic compression of the soil skeleton. Because of the condition of insular air saturation [24,25], changes in the degree of saturation occur with suction remaining at zero [8]. The decrease in

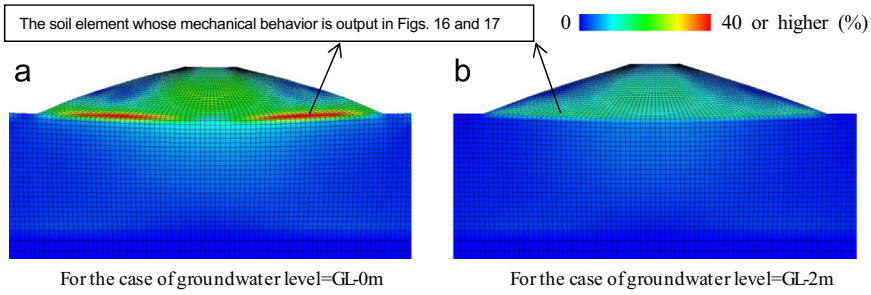

Fig. 12. Comparison of shear strain distributions immediately after the earthquake. (a) For the case of groundwater level=GL-0m. (b) For the case of groundwater level=GL-2m.

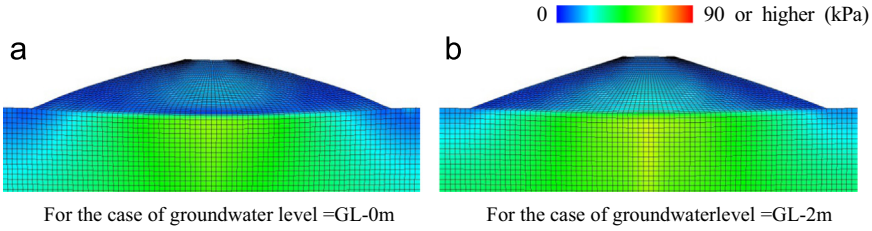

Fig. 13. Comparison of mean skeleton stress distributions immediately after the earthquake. (a) For the case of groundwater level=GL-0m. (b) For the case of groundwater level=GL-2m.

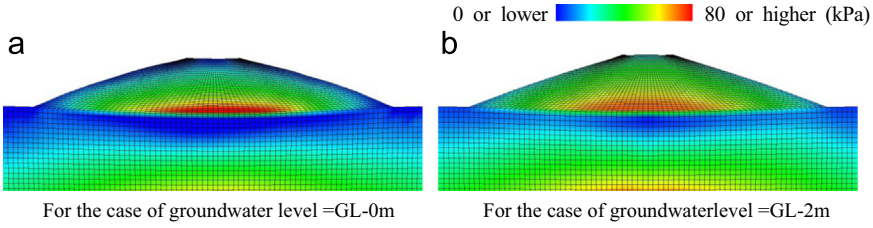

Fig. 14. Comparison of excess pore water pressure distributions immediately after the earthquake. (a) For the case of groundwater level=GL-0m. (b) For the case of groundwater level=GL-2m.

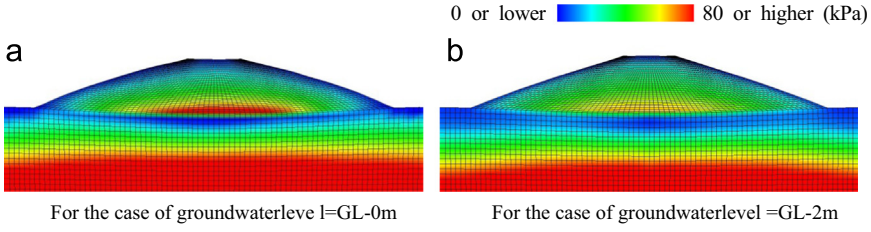

Fig. 15. Comparison of pore air pressure distributions immediately after the earthquake. (a) For the case of groundwater level=GL-0. (b) For the case of groundwater level=GL-2m.

the mean skeleton stress in the case of GL-2m was small compared with the case of GL-0m. The reason for this lies in the fact that in addition to the mean skeleton stress being large (as mentioned in Section 3), the degree of saturation of 65% means the existence of a large volume of air that can be compressed instantaneously even under short-term external forces due to earthquakes. The fact that the air was compressed can be confirmed by the increase in the degree of saturation, the decrease in volume, and the increase in air pressure.

Let us proceed to discuss the phenomenon of the rise in water level after the earthquake. Fig. 18 shows the distribution of the degree of saturation in the case of GL-0m. Fig. 18(a) is a contour diagram before the earthquake, and Fig. 18(b) is one 30 days after the earthquake, when the water level is at its maximum. In addition, assuming that the phreatic line is the one formed by joining the soil elements whose degree of saturation is equal to the maximum degree of saturation of 99%, contour diagrams generated by setting the maximum and minimum values to $\pm 0.5\%$ of 99% are also shown. It can be seen from Fig. 18 that the water level within the embankment rises after the earthquake. Fig. 19 shows the distribution of the degree of saturation in the case of GL-2m (a) before the earthquake and (b) 50 days after the earthquake, i.e. when the water level is at its maximum. Although the water level rises in this case (GL-2m) too, no phreatic line appeared within the embankment because the water level was low originally. The water level, which rose once, returned to its original level 1–2 years after the earthquake because of the total water head boundaries set at the ground and embankment surfaces.

Taking the case of GL-0m as an example, the process of the water level rise is discussed below. The mechanism is also discussed in the next section using the results of a simpler analysis. Figs. 20–23 depict the post-seismic distributions of the excess pore water pressure, pore air pressure, mean skeleton stress and degree of saturation, respectively. Comparison with the distributions immediately after the

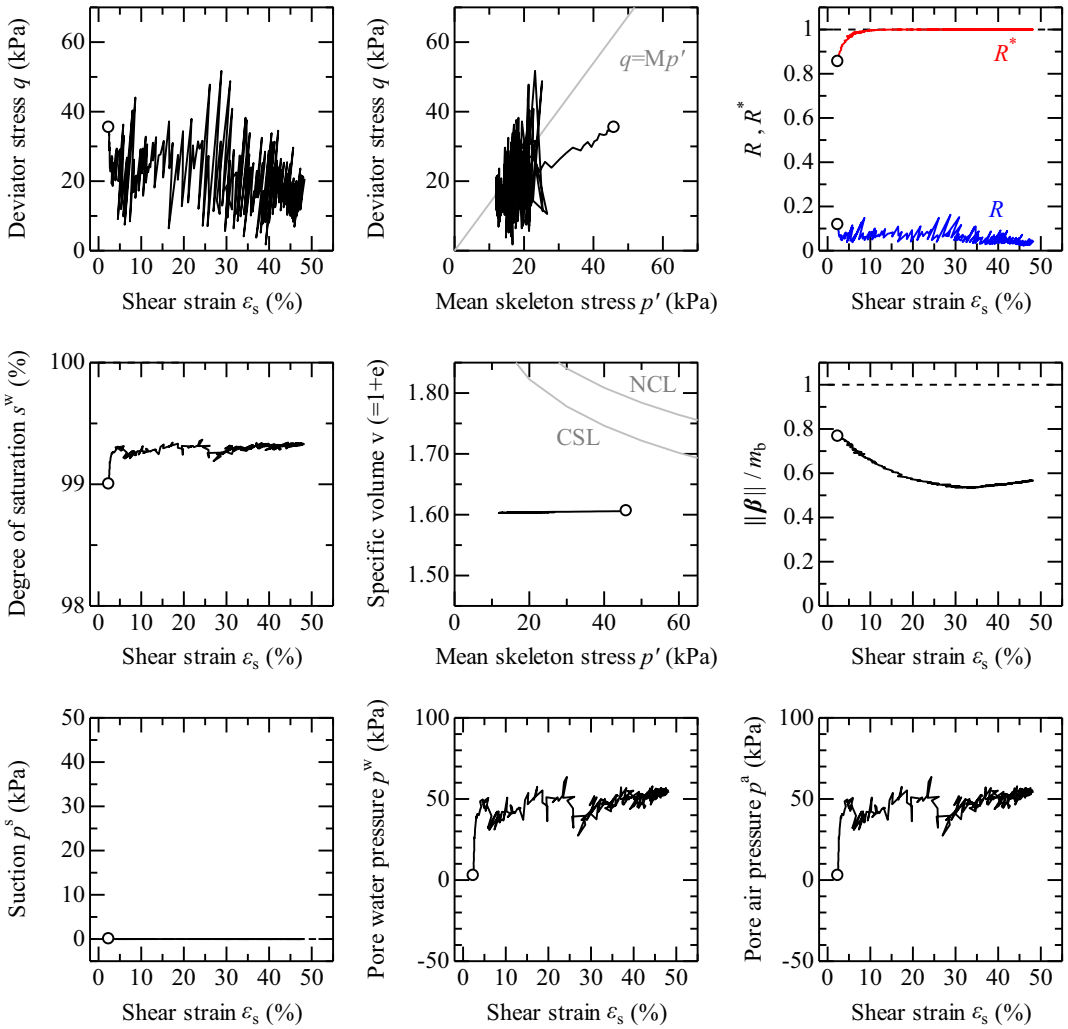

Fig. 16. Co-seismic mechanical behavior of a soil element for the case of groundwater level=GL-0m.

earthquake (Figs. 13–15) shows that the mean skeleton stress of the embankment recovered 12 h after the earthquake. Dissipation of the excess pore water pressure and decrease of the pore air pressure can be observed too. As explained in Section 2.2, the coefficient of air permeability is greater than that of water permeability up to a degree of saturation of 98.6%. Furthermore, the excess pore water pressure distribution and pore air pressure distribution in the embankment immediately after the earthquake exhibit similarity. Accordingly, air is exhausted from the embankment surface before water drainage occurs. Recovery of the mean skeleton stress, lowering of the air pressure and lowering of the water pressure occur as a result of this air exhaust. The distribution of the degree of saturation 12 h after the earthquake shows that the degree of saturation increased at the base of the embankment and that the phreatic area expanded. This is because the excess pore water pressure dissipates in areas of the embankment except the settlement-induced saturation area because of air exhaust. Consequently, water flows to such areas from the settlement-induced saturation area, in which a significant increase in the excess pore water occurred. With respect to the clayey ground, however, the excess pore water pressure which rose during the earthquake due to plastic volumetric compression remains unchanged even 12 h after the earthquake. This creates a hydraulic gradient between the clayey ground and the embankment, in which the excess pore water pressure has dissipated. This hydraulic gradient causes delayed flow of water from the ground to the embankment. As a consequence, there is further expansion of the above phreatic area at 30 days after the earthquake. At 30 days after the earthquake, it can also be observed that the excess pore water pressure in the clayey ground dissipated and that the mean skeleton stress recovered.

5. Mechanism of rise in water level within the embankment after the earthquake

Finally, analysis was carried out using very simple conditions in order to investigate the phenomenon of a rise in water level in the unsaturated embankment after the earthquake with particular focus on clarifying the source of the water flowing into the embankment. Fig. 24 shows the analyzed cross section. The analysis (two-dimensional plane strain condition) was carried out using a simple finite element mesh made up of single transverse elements. As hydraulic boundary conditions, all boundaries (top, bottom, left and right) were made undrained, shutting out exchange of water between the analyzed cross section and the outside. As air boundary conditions, the top end was set as an exhausted boundary, with all other boundaries being set in the unexhausted condition. The embankment loading process was not calculated as a part of this analysis so that the results of the analysis could be comprehended more easily. The ground condition, including the embankment, was set so as to satisfy beforehand the equilibrium of force. Seismic response analysis was performed assuming this condition to be the initial condition. The initial groundwater level was set at the boundary between the clayey

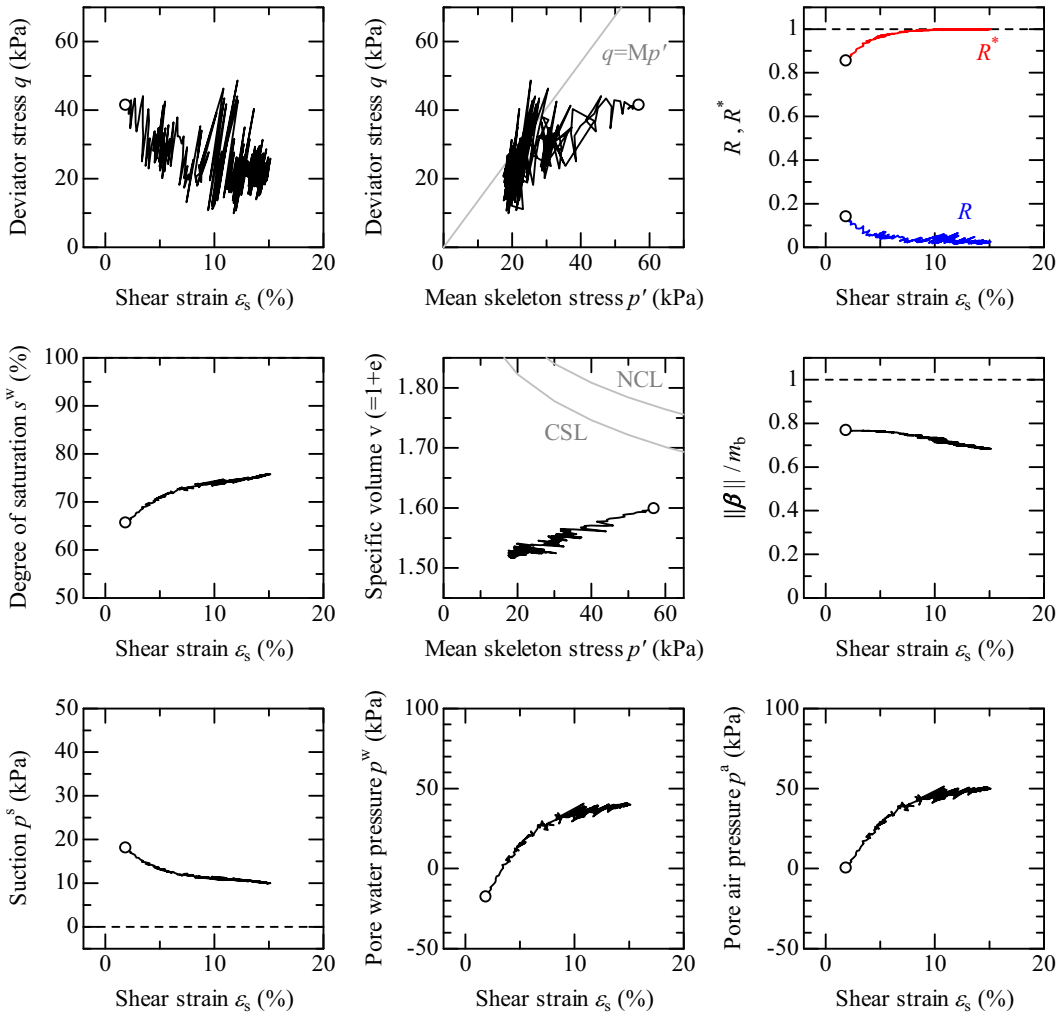

Fig. 17. Co-seismic mechanical behavior of a soil element for the case of groundwater level=GL-2m.

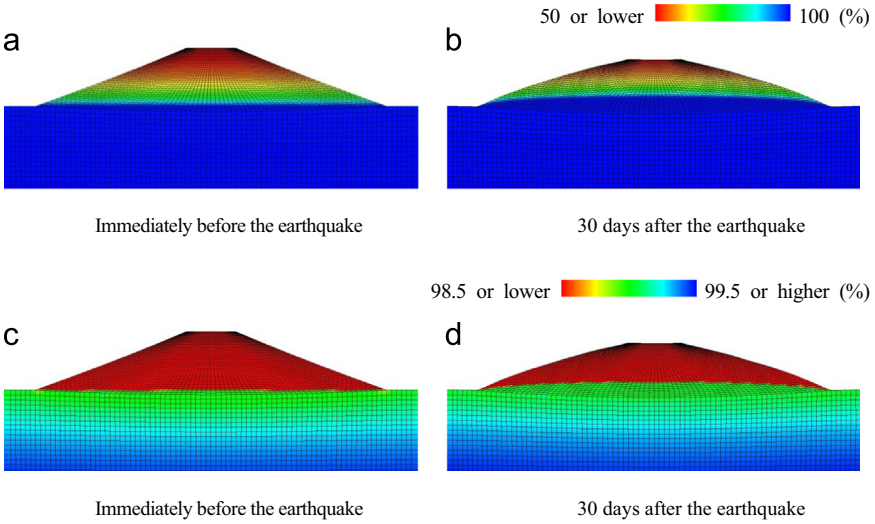

Fig. 18. Distributions of the degree of saturation after the earthquake, showing the rise in water level: a phreatic line is formed within the embankment. (For the case of groundwater level=GL-0m). (a) Immediately before the earthquake. (c) Immediately before the earthquake. (b) 30 days after the earthquake. (d) 30 days after the earthquake.

ground and the embankment. The values of the material constants used were the same as those employed earlier. As geometric boundary conditions and mechanical boundary conditions, only the vertical direction of the bottom end was made fixed; the horizontal direction of the bottom end was set as a viscous boundary, and the left and right ends were made periodic boundaries. The seismic wave shown in Fig. 5 was input to the lower end in the same manner as earlier.

Fig. 25 depicts the distributions of the degree of saturation, pore water pressure and amount of water absorbed/drained. Comparison of the distributions of the degree of saturation before and after the

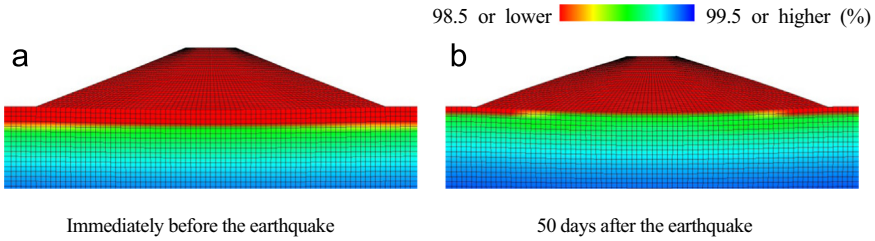

Fig. 19. Distributions of the degree of saturation after the earthquake, showing the rise in water level: There is no formation of phreatic lines within the embankment. (For the case of groundwater level=GL-2m). (a) Immediately before the earthquake. (b) 50 days after the earthquake.

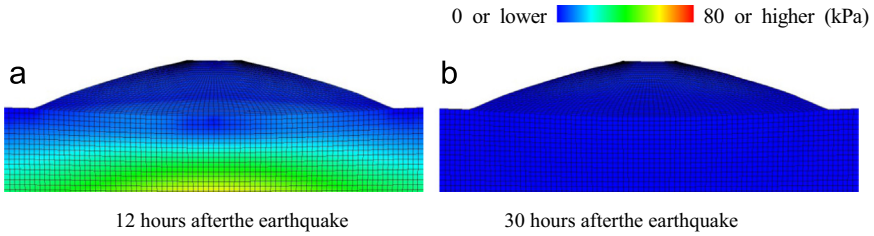

Fig. 20. Excess pore water pressure distributions after the earthquake. (For the case of groundwater level=GL-0m). (a) 12 h after the earthquake. (b) 30 days after the earthquake.

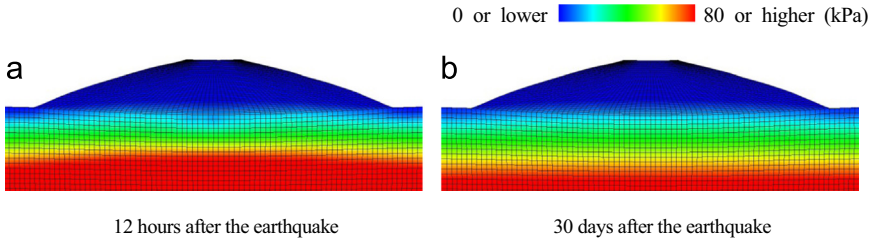

Fig. 21. Pore air pressure distributions after the earthquake. (For the case of groundwater level=GL-0m). (a) 12 h after the earthquake. (b) 30 days after the earthquake.

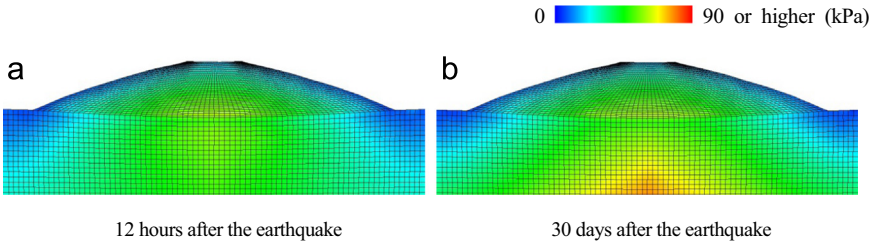

Fig. 22. Mean skeleton stress distributions after the earthquake. (For the case of groundwater level=GL-0m). (a) 12 h after the earthquake. (b) 30 days after the earthquake.

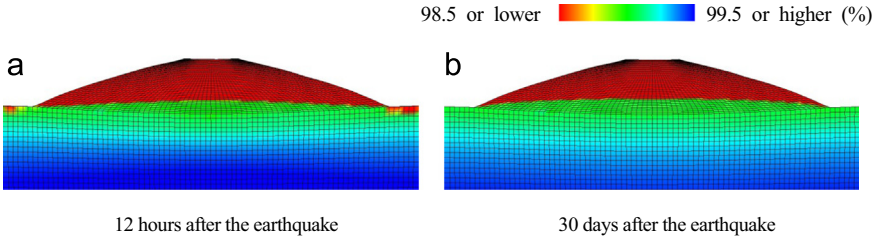

Fig. 23. Distributions of the degree of saturation after the earthquake. (For the case of groundwater level=GL-0m). (a) 12 h after the earthquake. (b) 30 days after the earthquake.

earthquake in Fig. 25(a) shows that the water level rose after the earthquake even though no water was supplied from the outside. An increase in the static water pressure after the earthquake due to the rise in water level can be seen in Fig. 25(b) too. However, in contrast to the case described in Section 4 above, the water level does not return to its original position because all boundaries were set as undrained ones. The amount of water absorbed/drained shown in Fig. 25(c) is the volume (cm^3) of water absorbed/drained calculated per meter of depth, assuming it to be zero in the initial condition before the earthquake. This figure shows that water absorption occurs mainly in the part of the embankment where the water level rose and that drainage takes place from the base of the embankment and the clayey

ground, where the degree of saturation is high. From these analytical results, the phenomenon of a rise in water level could be explained as follows. For one-dimensional consolidation of saturated soil with the top end being in the drained condition and the bottom end being in the undrained condition, since the amount of ground settlement is equal to the amount of water drained from the ground, the level of the supernatant water produced by the drainage during consolidation would be equal to the height of the ground before consolidation if the effects of rain and evaporation are not taken into account. In the current analysis, the degrees of saturation of the base of the embankment and the clayey ground were high enough to allow them to be considered as saturated soils, and the external forces exerted by the earthquake caused consolidation. The drained water produced by the consolidation is not supernatant but is supplied to the unsaturated soil elements in the higher parts of the embankment. Unlike in the case of supernatant water only, soil particles are present in the soil elements. Therefore, the water level will rise by an extra amount equivalent to the volume of the soil particles. For a given amount of drained water produced by consolidation, the water level will be higher if the pores in the soil elements of the upper parts are smaller and the soil particles are more densely packed. If the pores are infinitely small, the water level rise will be infinite in theory. It can therefore be inferred that the above phenomenon may have occurred during the off the Pacific coast of Tohoku Earthquake in some levees in which the measured groundwater levels within the levees became higher than the surrounding ground surface 50 days after the earthquake and then decreased after about 75 more days, as has been reported by Sasaki et al. [1]. Consolidation is produced by not only seismic forces but also embankment loading. In Section 3, during embankment construction, the analysis showed the water level rise although the figures were omitted.

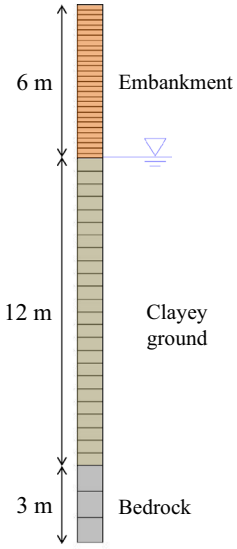

Fig. 24. Cross section used for one-dimensional analysis carried out to understand the phenomenon of a rise in water level.

The phenomenon of a rise in water level shown in this section cannot be expressed if the soil is assumed to be an elastic body. The results of such an analysis, however, are omitted here. A rise in water level that occurs as a result of external seismic forces causing consolidation drainage (plastic volumetric compression) to take place in embankment bases and clayey grounds with high

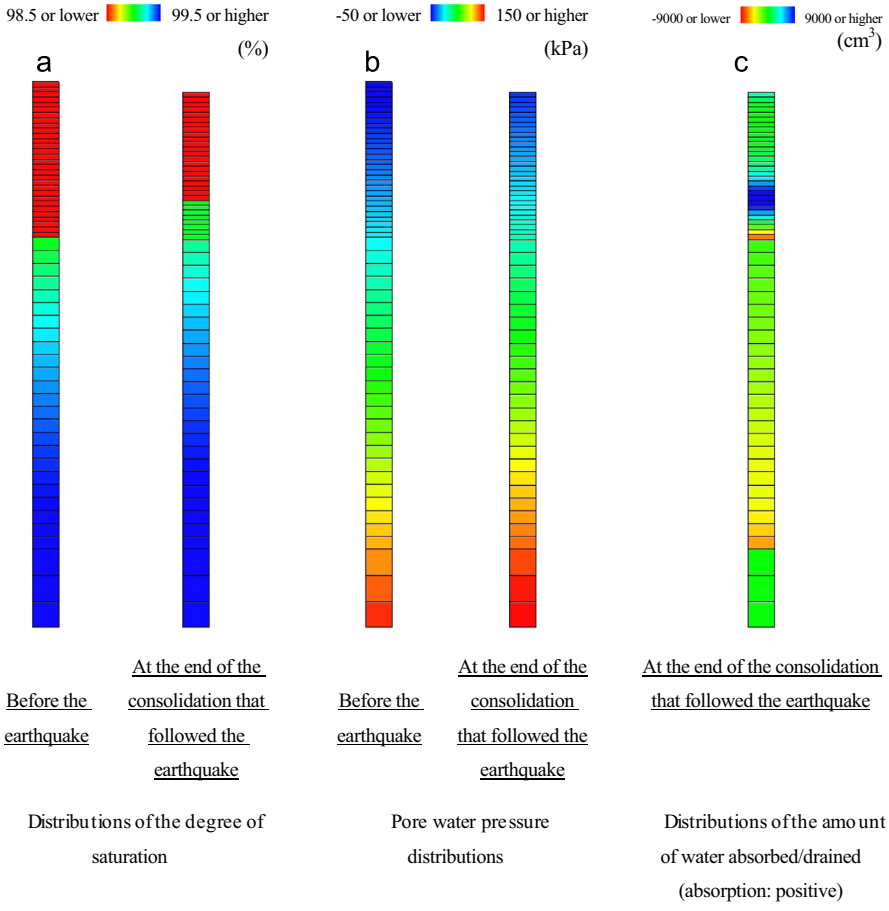

Fig. 25. Distributions of the degree of saturation, pore water pressure and amount of absorbed/drained water. (a) Distributions of the degree of saturation. (b) Pore water pressure distributions. (c) Distributions of the amount of water absorbed/drained (absorption: positive).

Fig. 26. Water outflow seen in a box culvert of a highway embankment on clayey ground affected by the Mid Niigata Prefecture Earthquake in 2004. (The earthquake occurred on 23 October 2004. These photographs were taken on 5 November 2004).

degrees of saturation can be expressed by treating soil as an elasto-plastic body and carrying out analysis for a three-phase system.

6. Conclusion

In order to clarify the mechanism of the collapse of many river levees on clayey ground caused by the 2011 off the Pacific coast of Tohoku Earthquake, the behavior of an unsaturated embankment on clayey ground during its construction, during an earthquake and after the earthquake was simulated using the soil-water-air coupled finite deformation analysis code [8] under very simple conditions, with attention being focused on the effect of groundwater level. During embankment construction, the mean skeleton stress is smaller in the case of a high groundwater level (GL-0m) compared with the case of a low groundwater level (GL-2m), and an settlement-induced saturation area is created at the base of the embankment. As a result, during the earthquake, it was shown that large shear deformation centering around the embankment base occurs in the case of the high groundwater level. In addition, it was made clear that in the case of the high groundwater level, a phreatic line is formed temporarily within the embankment. The results of this study showing the difference in mechanical behavior due to groundwater level differences are in agreement with the reported damage caused by the 2011 off the Pacific coast of Tohoku Earthquake. The knowledge obtained through this study is outlined below specifically.

Behavior during embankment construction:

(1) Due to the manner in which the total water head is assigned, the water pressure when consolidation ends is higher in the case of a high groundwater level compared with the case of a low groundwater level. As a result, the mean skeleton stress is low and the degree of saturation is high in the former case.
(2) Because of consolidation settlement of the clayey ground resulting from embankment loading, soil elements that sink below the groundwater level exhibit degrees of saturation greater than the maximum degree of saturation and an settlement-induced saturation area is formed. The current analysis indicates that an settlement-induced saturation area approximately 50 cm thick forms directly below the center of the crown of the embankment in the case of the groundwater level being GL-0m.

Behavior during and after the earthquake

(3) In the case of the high groundwater level, high (positive) excess pore water pressure and pore air pressure are generated in the settlement-induced saturation area at the embankment base, resulting in a significant decrease in the mean skeleton stress. The current analysis in the case of GL-0m showed that the settlement of the crown of the embankment during the earthquake is more than 1 m. Most of this settlement occurs in the embankment part.
(4) When the groundwater level is low, the mean skeleton stress is large compared with that when the groundwater level is high. In addition, the degree of saturation of the embankment is low, and a large amount of air, which is highly compressible, is present. As a result, the deformation that occurs during the earthquake is small.
(5) As a result of the air being exhausted from the embankment surface after the earthquake, both the pore air pressure and the pore water pressure within the embankment decrease, and the mean skeleton stress recovers.
(6) Due to the dissipation of the excess pore water pressure in the within embankment as described in (5) above, there is a flow of water toward the unsaturated embankment from the clayey ground and from the settlement-induced saturation area that exhibited an increase in excess pore water pressure due to plastic compression, and the groundwater level rises. Particularly in the case of the high groundwater level (GL-0m), a phreatic line is formed temporarily within the embankment.
(7) It is possible to express this phenomenon of a rise in water level by carrying out analysis for a three-phase system in addition to treating the soil skeleton as an elasto-plastic body, allowing description of plastic volume changes.

Fig. 26 shows water outflow from a weep hole as seen in a box culvert of a highway embankment on clayey ground affected by the Mid Niigata prefecture Earthquake in 2004. Practicing engineers have testified that they believe groundwater in unsaturated earth structures rose after the earthquake because water outflow was not observed at ordinary times. Groundwater level increase followed by decrease after an earthquake has recently been reported [26] and plastic volume compression/expansion of soil explained in Section 5 must be one of the mechanisms. In future work, the authors intend to verify this phenomenon experimentally, develop methods of assessing the seismic stability of similar structures, and formulate the principles of countermeasures.

Acknowledgments

Aid for this research was received from the Japan Society for the Promotion of Science (JSPS) under its "*KAKENHI*" (Grants-in Aid for Scientific Research) program (*KAKENHI* reference number 25249064) and from the Ministry of Land, Infrastructure, Transport and Tourism of Japan under its River Levee Technology Research and Development Program (Principal Investigator: Takeshi Kodaka; Fiscal years: 2012-2014). Clay soil specimens sampled from the *Narusegawa* river were kindly provided by Professor Motoki Kazama of Tohoku University,

and photographs of highway embankments affected by the Mid Niigata Prefecture Earthquake were provided by Mr. Motohiro Inagaki of Central Nippon Expressway Company (NEXCO Central). We wish to extend our thanks to the above institutions and individuals.

Appendix-A1. Method of assigning the initial pore water pressure distribution

Assume that the ground water surface is positioned at the vertical coordinate $z = z^{w}_{HW}$ (upward direction: positive) and that the water pressure is $p^{w} = p^{w}_{HW}$ at $z = z^{w}_{HW}$. In this condition, the static water pressure $p^{w}(z)$ at $z = z$ is given by the following equation, where ρ^{w} is the density of water, and g is the gravitational acceleration.

$$p^{w}(z) = p^{w}_{HW} + \int_{z}^{z^{w}_{HW}} \rho^{w} g dz' \tag{A1}$$

If ρ_0 ($=1.0$ g/cm^3) is the density of water when the water pressure is 0 kPa, then the following equation expresses the density $\rho^{w}(p^{w})$ when the water pressure is $p^{w} = p^{w}$ under the condition that temperature changes are not taken into consideration.

$$\rho^{w}(p^{w}) = \rho_0 \exp\left(\frac{p^{w}}{K_w}\right) \tag{A2}$$

In the above equation, K_w is the bulk modulus of water and is a constant.

Using Eq. (A2) to solve Eq. (A1) yields the equation below.

$$p^{w}(z) = -K_w \ln\left\{\exp\left(-\frac{p^{w}_{HW}}{K_w}\right) + \frac{\rho_0 g\left(z - z^{w}_{HW}\right)}{K_w}\right\} \tag{A3}$$

Eq. (A3) was utilized in this paper to assign the initial pore water pressure distribution.

Appendix-B2. Method of assigning the initial pore air pressure distribution in locations shallower than the ground water level

Assuming the air pressure to be $p^{a} = p^{a}_{0}$ at the vertical coordinate $z = z^{a}_{0}$ (upward direction: positive) and taking into consideration the weight of air itself, the air pressure $p^{a}(z)$ at $z = z$ is expressed by Eq. (A4), where ρ^{a} is the density of air.

$$p^{a}(z) = p^{a}_{0} + \int_{z}^{z^{a}_{0}} \rho^{a} g dz' \tag{A4}$$

Assuming that air behaves according to the equation of state of ideal gas, the density of the air $\rho^{a}(p^{a})$ when the air pressure is $p^{a} = p^{a}$ will be expressed by the equation below.

$$\rho^{a}(p^{a}) = \frac{1}{\overline{R}\Theta}(p_0 + p^{a}) \tag{A5}$$

In the above equation, p_0 denotes 1 atm ($=101.325$ kPa) and Θ is the absolute temperature. $\overline{R}$ is the gas constant divided by the mean molecular weight of air, and its value is 287.04 m^2/s^2/K. Since the equation of state of ideal gas requires the absolute pressure to be used, p_0 has been added to p^{a} in the above equation.

The following equation is obtained by solving Eq. (A4) using Eq. (A5).

$$p^{a}(z) = (p_0 + p^{a}_{0}) \exp\left\{\frac{g}{\overline{R}\Theta}\left(z^{a}_{0} - z\right)\right\} - p_0 \tag{A6}$$

Note that Eq. (A6) does not take temperature changes into consideration. Eq. (A6) was utilized in this paper to assign the initial pore air pressure distribution at locations shallower than the groundwater level, assuming that the air pressure at the initial ground surface was 0 kPa (i.e. $z^{a}_{0} = 15$m, $p^{a}_{0} = 0$ kPa).

Appendix-C3. Method of assigning the distribution of initial degree of saturation at locations deeper than the ground water level

At locations deeper than the ground water level, suction is zero, and the pore air, which is entrained into the pore water in the form of bubbles, is in a state of insular air saturation [24,25]. Assuming that the degree of saturation is $s^{w} = s^{w}_{0}$ when the pore water pressure (and pore air pressure) is $p^{w} = p^{w}_{0}$, calculations are performed under the premise that the pore water and pore air in the same state as above are compressed according to the rise in pressure in the depth direction. Therefore, the degree of saturation $s^{w}(p^{w})$ when the pore water pressure (and pore air pressure) is $p^{w} = p^{w}$ can be expressed by Eq. (A7) below using the pore water density $\rho^{w}(p^{w})$ and pore air density $\rho^{a}(p^{w})$ when $p^{w} = p^{w}$, and using the pore water density ρ^{w}_{0} and pore air density ρ^{a}_{0} when $p^{w} = p^{w}_{0}$.

$$s^{w}(p^{w}) = \frac{\frac{\rho^{w}_{0}}{\rho^{w}(p^{w})}}{\frac{\rho^{w}_{0}}{\rho^{w}(p^{w})} + \frac{\rho^{a}_{0}}{\rho^{a}(p^{w})}\frac{1 - s^{w}_{0}}{s^{w}_{0}}} \tag{A7}$$

The distribution of the initial degree of saturation at locations deeper than the ground water level was assigned using the equation that was obtained by substituting Eqs. (A2) and (A5) into Eq. (A7). In this study, under the premise that the maximum degree of saturation s^{w}_{max} occurs when the pore water pressure (and pore air pressure) is 0 kPa, the values $p^{w}_{0} = 0$ kPa and $s^{w}_{0} = s^{w}_{max}$ were used.

References

[1] Sasaki Y, Towhata I, Miyamoto K, Shirato M, Narita A, Sasaki T, Sako S. Reconnaissance report on damage in and around river levees caused by the 2011 off the Pacific coast of Tohoku earthquake. Soils Found 2012;52(5):1016–32. http://dx.doi.org/10.1016/j.sandf.2012.11.018.

[2] The Japanese Geotechnical Society. Geo-hazards during earthquakes and mitigation measures. Lessons and recommendations from the 2011 Great East Japan earthquake (second report); 2012 [in Japanese].

[3] Report of the technical committee for study of restoration techniques of Levees along the Kitakamigawa River and other rivers. Tohoku Regional Development Bureau, Ministry of Land, Infrastructure, Transport and Tourism; 2012 [in Japanese] ⟨http://www.thr.mlit.go.jp/Bumon/B00097/K00360/taiheiyouokijishinn/kenntoukai/houkokusho.pdf⟩ [accessed on 27.6.15].

[4] Sasaki Y, Oshiki H, Nishikawa J. Embankment failure caused by the Kushiro-Oki earthquake of January 15, 1993. In: Proceedings of the session publication during the 13th ICSMGE. Delhi; 1994, p. 61–8.

[5] Uzuoka R, Semba K. Numerical analysis of liquefaction in a river levee on soft cohesive ground. J Disaster Res 2012;7(6):711–7.

[6] Okamura M, Tamamura S, Yamamoto R. Seismic stability of embankments subjected to pre-deformation due to foundation consolidation. Soils Found 2013;53(1):11–22 http://dx.doi.org/10.1016/j.sandf.2012.07.015.

[7] Sub-committee on Levees, Committee of Geotechnical Engineering, JSCE. Committee reports and abstracts of the first symposium on levee technologies viewed from the perspective of geotechnical engineering; 2013 [in Japanese] ⟨http://www.cee.ehime-u.ac.jp/~gm/Dike%20symposium.pdf⟩ [accessed on 27.6.15].

[8] Noda T, Yoshikawa T. Soil–water–air coupled finite deformation analysis based on a rate-type equation of motion incorporating the SYS Cam-clay model. Soils Found 2015;55(1):45–62. http://dx.doi.org/10.1016/j.sandf.2014.12.004.

[9] Noda T, Asaoka A, Nakano M. Soil–water coupled finite deformation analysis based on a rate-type equation of motion incorporating the SYS Cam-clay model. Soils Found 2008;48(6):771–90. http://dx.doi.org/10.3208/sandf.48.771.

[10] Asaoka A, Noda T, Yamada E, Kaneda K, Nakano M. An elasto-plastic description of two distinct volume change mechanisms of soils. Soils Found 2002;42(5):47–57. http://dx.doi.org/10.3208/sandf.42.5_47.

[11] Noda T, Asaoka A, Yamada S. Some bearing capacity characteristics of a structured naturally deposited clay soil. Soils Found 2007;47(2):285–301. http://dx.doi.org/10.3208/sandf.47.285.

[12] Nakano M, Yamada E, Noda T. Ground improvement of intermediate reclaimed land by compaction through cavity expansion of sand piles. Soils Found 2008;48(5):653–71. http://dx.doi.org/10.3208/sandf.48.653.

[13] Noda T, Takeuchi H, Nakai K, Asaoka A. Co-seismic and post-seismic behavior of an alternately layered sand–clay ground and embankment system

accompanied by soil disturbance. Soils Found 2009;49(5):739–56. http://doi.org/10.3208/sandf.49.739.
[14] Takaine T, Tashiro M, Shiina T, Noda T, Asaoka A. Predictive simulation of deformation and failure of peat-calcareous soil layered ground due to multi-stage test embankment loading. Soils Found 2010;50(2):245–60. http://doi.org/10.3208/sandf.50.245.
[15] Tani K, Matsushita K, Hashimoto T, Yamamoto A, Takeuchi H, Noda T, Kiku H, Obayashi J, Kiyota T. Mitigation of liquefaction-induced damage to residential houses by surface ground improvement and its cost evaluation. Jpn Geotech J 2014;9(4):533–53 [in Japanese].
[16] van Genuchten MT. A closed-form equation for predicting the hydraulic conductivity of unsaturated soils. Soil Sci Soc Am J 1980;44(5):892–8.
[17] Carsel RF, Parrish RS. Developing joint probability distribution of soil water retention characteristics. Water Resour Res 1988;24(5):755–69.
[18] Mualem Y. A new model for predicting the hydraulic conductivity of unsaturated porous media. Water Resour Res 1976;12(3):513–22.
[19] Sakai T, Nakano M. Interpretation of the effect of compaction on the mechanical behavior of embankment materials based on the soil skeleton structure concept. In: Proceedings of the 18th international conference on soil mechanics and geotechnical engineering; 2013, p. 1179–82.
[20] Midorikawa S. Prediction of isoseismal map in the Kanto plain due to hypothetical earthquake. J Struct Eng 1987;33B:43–8 [in Japanese].
[21] Lysmer J, Kuhlemeyer RL. Finite dynamic model for infinite media, 95. ASCE; 1969. p. 859–77.
[22] Joyner WB, Chen ATF. Calculation of nonlinear ground response in earthquakes. Bull Seism Soc Am 1975;65(5):1315–36.
[23] Jommi C. Remarks on the constitutive modelling of unsaturated soils. In: Tarantino A, Mancuso C, editors. Experimental evidence and theoretical approaches in unsaturated soils. Balkema; 2000. p. 139–53.
[24] Bear J. Hydraulics of groundwater. New York: McGraw-Hill; 1979. p. 190–224.
[25] Kohgo Y, Nakano M, Miyazaki T. Theoretical aspects of constitutive modeling for unsaturated soils. Soils Found 1993;33(4):49–63. http://dx.doi.org/10.3208/sandf1972.33.4_49.
[26] Fuyuki H, Ichiro N. Seismic ground motion, tsunami damage, and change of groundwater level in the southernmost of Ehime prefecture (Ainan-town) caused by the 1854 Ansei Nankai Earthquake: usefulness of document written by a village headman and potential for estimation of crustal deformation, Zisin. J Seismol Soc Jpn 2015;68:107–24 [in Japanese].